Monte Carlo studies of equilibrium and growth shapes of a crystal

Yukio Saito and Tsuyoshi Ueta
Department of Physics, Keio University, 3-14-1 Hiyoshi, Kohoku-ku, Yokohama 223, Japan
(Received 21 March 1989)

The equilibrium and growth morphology of a crystal in a diffusion field are studied by means of a lattice-gas model in a unified way. In a closed system the crystal takes an equilibrium form, and its shape and size in two dimensions agree with those expected from the exact solutions of the corresponding Ising model. In an open system where a crystal is in contact with a gas reservoir, the crystal grows steadily. For a small crystal or at a small chemical potential difference $\Delta\mu$ between the gas and the crystal, the growth form is polygonal. Its growth rate and the size are interpreted by a single nucleation and growth mechanism. On increasing $\Delta\mu$ or for a large crystal, it becomes dendritic. Further increase of $\Delta\mu$ results in a fractal aggregate, which is, however, "compact" in a large scale due to the finiteness of the gas density.

I. INTRODUCTION AND THE MODEL

Pattern formations in various diffusion fields have been investigated recently as a typical problem of nonequilibrium statistical physics.[1] Even though bulk systems follow the same diffusion equation or its static limit, i.e., the Laplace equation, patterns vary from one system to another: In a unidirectional solidification from solution a crystal interface takes a regular form as an array of cells, cusps, or dendrites.[1,2] When a dendrite is isolated and free, it has a parabolic tip with almost regular sidebranches.[1-3] In a Hele-Shaw channel a viscous finger is regular,[4] whereas in a circular geometry fingers show tip splitting and become ramified.[5,6] In the limit of vanishing interfacial energy, patterns become fractal. A typical fractal pattern is found in a diffusion-limited aggregation (DLA), whose structure is characterized by a fractal dimension D_f.[7]

The main cause of these variations is the difference in a boundary condition, more specifically, it is the effect of surface tension. Surface tension suppresses the instability caused by the diffusion field, and its anisotropy selects the working point of the growth pattern.[8-12] In macroscopic theories of the unidirectional solidification,[13-15] the free dendrite,[8-12] and the viscous fingers,[16] the surface tension is treated phenomenologically and is given as an input parameter. In the DLA problem, the effect of surface tension is replaced by an artificial algorithm in the numerical simulation.[17] On the other hand, the surface tension by itself is interesting in relation to equilibrium phase transitions, namely, a roughening transition of a particular crystal face[18] and a faceting transition of an equilibrium morphology.[19] In these cases, microscopic treatment of the surface tension is necessary. In this paper we propose a simple model of a crystal growing in a diffusion field, which considers the effect of the surface tension microscopically, such that the equilibrium and the growth forms of the crystal are treated in a unified way.

In order to get a simple model, we interpret that the gas and the solid phases consist of their respective atoms: A gas atom is mobile to give an entropy contribution of the chemical potential, whereas a solid atom is immobile but its chemical potential has the contribution from the energy. The situation is further simplified by considering a lattice system, where the space is divided into discrete lattice points. Each lattice site can be occupied by a solid atom, by a gas atom, or can be empty. Double occupancy of a lattice site is forbidden. Figure 1 represents an instantaneous configuration of gas and solid atoms on a square lattice. Since the system has fourfold symmetry, we consider only an upper-right quarter of a crystal nucleus in the positive x and y regions. In order to fix the

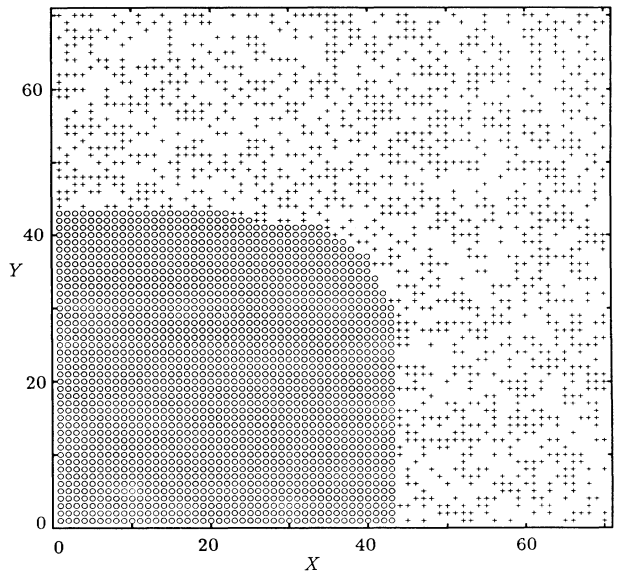

FIG. 1. Atomic configuration at $T/J=0.3$, $\mu_s/T=-1.0$, taken at the 30 000th MCS. The vessel size is $\Omega=70\times70$, and among $N=56\times56$ atoms, $N_s=1767$ atoms are in a solid state ($\circ$) and $N_g=1369$ atoms are in a gaseous state ($+$).

center of the mass at the origin, a skewed boundary condition is assumed so that the x and y axes are contiguous to each other.

With each solid atom an energy gain $\mu_s(<0)$ is associated, while a gas atom gains the entropy by exchanging its position with a neighboring empty site. This exchange process also mimics the diffusion in a gas phase. The effect of the surface tension can be incorporated by an energy cost of a value $2J>0$ in breaking a solid-solid nearest-neighbor bond. These energetics are summarized in a Hamiltonian

$$H=2J\sum_{\langle i,j\rangle}[C_i(1-C_j)+(1-C_i)C_j]+\mu_s\sum_i C_i\ , \tag{1}$$

where the first summation runs over all the nearest-neighbor pairs, and the crystallization order parameter C_i on an ith lattice site is unity when it is occupied by a solid atom and vanishes otherwise. In terms of an Ising spin variable $S_i\equiv 2C_i-1=\pm 1$, the Hamiltonian reduces to that of a ferromagnetic Ising model in a field,

$$H=-J\sum_{\langle i,j\rangle}S_iS_j+(\mu_s/2)\sum_i S_i+(\Omega/2)(zJ-\mu_s)\ . \tag{2}$$

Here the volume Ω being the number of the total lattice sites and z the coordination number.

Monte Carlo simulations[20] have been performed for the lattice-gas model, Eq. (1), to obtain crystal shapes. Stochastic evolution of the system consists of the following steps. Every gas atom hops freely from a lattice site to one of its nearest neighbors, unless it is occupied. When a gas atom diffuses to come into contact with solid atoms, it crystallizes with a probability W. Inverse to this crystallization process is an evaporation, where a solid atom at an interface tries to turn into a gas atom. These crystallization and evaporation processes at the interface should satisfy the detailed balance condition and we have adapted the heat-bath algorithm: The transition probability W for a process with an energy change ΔE at a temperature T is set to be $W(\Delta E)=[1+\exp(\Delta E/T)]^{-1}$.

Our process neglects the evaporation in the bulk crystal and solidification in the bulk of the gas phase, since our main concern is with the crystal morphology at low temperatures where these excitations in bulk phases are quite rare. This is the same assumptions for the solid-on-solid (SOS) model which simulates the thermal behavior of a singular interface.[18] The equilibrium shape of the SOS model has been simulated by the Monte Carlo method previously.[21,22] However, the SOS model is inappropriate for obtaining some types of growth forms as dendrite and fractal patterns, since it does not allow overhanging of the interface, which is essential for these morphologies.

We start a simulation with a solid nucleus situated in a closed vessel. Some solid atoms evaporate to a gas phase and diffuse away from the interface, but some gas atoms condense back. From this simulation we get an equilibrium form of the crystal.[21,22] Instead, if the system is expanded steadily by adding an atom reservoir with a prescribed gas density at the periphery of the system, the crystal continues to grow and we get a growth form. We consider a system on a square lattice. As for the roughening and faceting transitions, the two-dimensional (2D) system with a one-dimensional interface is not so interesting, due to the absence of phase transitions. However, since there are various exact results known in two dimensions, we consider it appropriate to start the study from 2D systems. In Sec. II we investigate the equilibrium form, and compare simulation results with the exact profiles. In Sec. III the variation in the growth form as a function of the chemical potential gain $|\mu_s|$ is studied. The relationship of the structures and the growth rate is also investigated.

II. EQUILIBRIUM SHAPE AND SIZE

Wulff's theorem states that an equilibrium shape of a crystal can be constructured from the orientation-dependent surface tension $\gamma(\theta)$.[23] Since our model, Eq. (1) corresponds to the Ising ferromagnet, Eq. (2), $\gamma(\theta)$ is exactly known for a square lattice[24] to be

$$\gamma(\theta)/T=|\cos\theta|\sinh^{-1}(\alpha|\cos\theta|)+|\sin\theta|\sinh^{-1}(\alpha|\sin\theta|)\ , \tag{3}$$

with

$$\alpha=(2/b)(1-b^2)^{1/2}[1+(\sin^2 2\theta+b^2\cos^2 2\theta)^{1/2}]^{-1/2}\ ,$$

$$b=2\sinh(2J/T)\cosh^{-2}(2J/T)\ .$$

Hereafter we take a temperature unit where the Boltzmann constant k_B is unity. The interface profile is then exactly represented in a parametric form by using Wulff's construction as

$$\begin{aligned}\lambda x&=\gamma(\theta)\cos\theta-\gamma(\theta)'\sin\theta\ ,\\ \lambda y&=\gamma(\theta)\sin\theta+\gamma(\theta)'\cos\theta\ ,\end{aligned} \tag{4}$$

where λ is a Lagrange multiplier which determines the crystal size, and the prime means the derivative by θ. The theoretical profile, Eq. (4) with Eq. (3), is compared with the simulated shape to test our simulation algorithms.

In Fig. 2 we show an averaged interface profile at temperatures (a) $T/J=0.3$ and (b) $T/J=0.6$. The interface is located at the position where an averaged degree of crystallization $\langle C\rangle$ is $\frac{1}{2}$. The average is performed over $2\sim 3\times 10^4$ Monte Carlo steps per site (MCS) for $T/J=0.6$ and over $3\sim 6\times 10^4$ MCS for $T/J=0.3$, disregarding the initial 10^4 MCS as an equilibration in every simulation. At each temperature, crystal shapes for various chemical potentials μ_s are similar but the size increases on increasing $|\mu_s|/T$. On heating the system the crystal shape becomes rounded. The temperatures simulated, $T/J=0.3$ and 0.6 are far below the Ising critical temperature $T_c/J=2/\ln(1+\sqrt{2})\approx 2.27$, and assure the absence of a hole creation in the crystal nucleus. Our simulation profiles agree with theoretical ones, Eq. (4) with Eq. (3), which are drawn by curves in Fig. 2 with an adjustment in the top height of the crystal.

In order to discuss the size of a nucleus, we assume that the crystal shape is scaled to the equilibrium form determined by Wulff's theorem. Suppose that in a vessel of volume Ω there are totally N atoms. Among them, N_s

solid atoms gather to form a solid nucleus, and the remaining $N_g = N - N_s$ gas atoms are distributed and diffuse in a free volume $\Omega - N_s$. The associated entropy of the gas phase is obtained to be

$$S_g = \ln[(\Omega - N_s)!/(N - N_s)!(\Omega - N)!] \ . \tag{5}$$

From our scaling assumption of the crystal shapes the interfacial energy scales to the linear dimension of the crystal $L = \sqrt{N_s}$, and a proportionality coefficient should be an averaged surface tension $\bar{\gamma}(T)$:

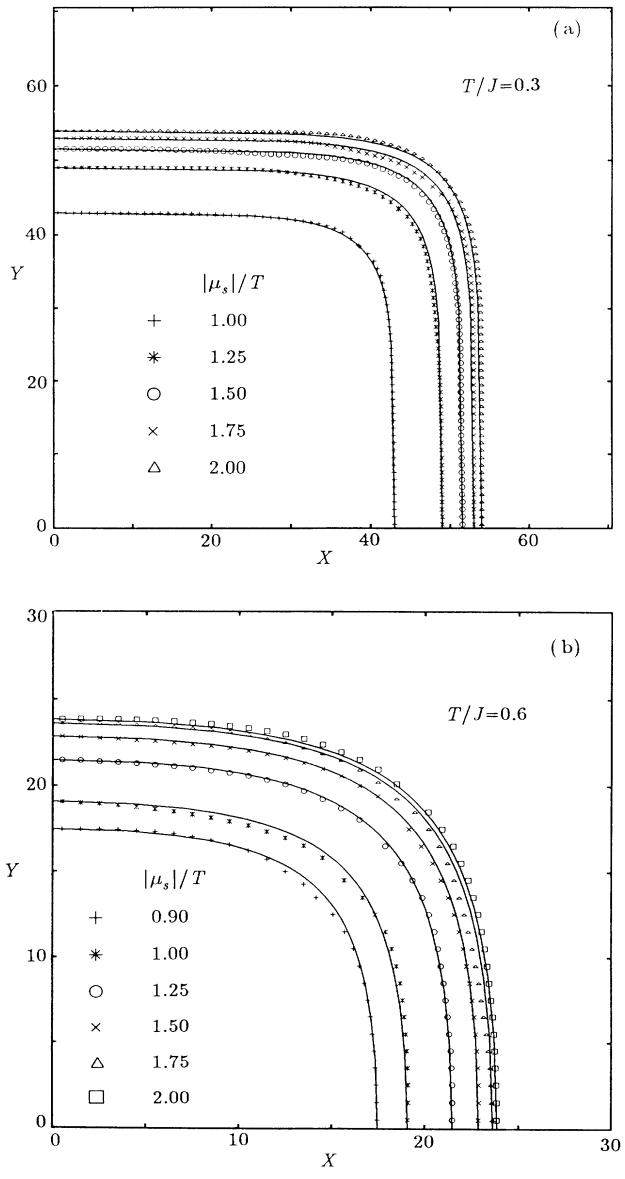

FIG. 2. Average interfacial profiles at (a) $T/J = 0.3$ and (b) $T/J = 0.6$ with various chemical potentials. Curves are the exact profile of the two-dimensional Ising model. The top height is fitted to the simulated profile.

$$\bar{\gamma}(T) = \int \gamma(\theta(s)) ds / 2 \left[\int y \, dx \right]^{1/2} , \tag{6}$$

where the integration is performed along the periphery s of the quarter of the crystal. Note that $\bar{\gamma}(T)$ depends only on a temperature and is independent of the system size N_s. Including the energy gain by crystallization $\mu_s N_s$, we get the total free energy

$$F(N_s) = 2\bar{\gamma}(T)\sqrt{N_s} + \mu_s N_s - TS_g \ . \tag{7}$$

A free-energy cost of the formation of a crystal nucleus of the size N_s is then given by

$$\begin{aligned} \Delta F(N_s) &\equiv F(N_s) - F(N_s = 0) \\ &= 2\bar{\gamma}(T)\sqrt{N_s} + \mu_s N_s \\ &\quad - T \left[(\Omega - N_s) \ln \frac{\Omega - N_s}{\Omega} - (N - N_s) \ln \frac{N - N_s}{N} \right. \\ &\quad \left. + N_s \ln \frac{N}{\Omega} \right] . \end{aligned} \tag{8}$$

The extremum of ΔF determines the critical radius via a relation

$$\begin{aligned} \frac{\partial \Delta F(N_s)}{\partial N_s} &= \bar{\gamma}(T)/\sqrt{N_s} + \mu_s - T \ln[(N - N_s)/(\Omega - N_s)] \\ &= \bar{\gamma}(T)/\sqrt{N_s} - \Delta\mu = 0 \ . \end{aligned} \tag{9}$$

Here $\Delta\mu \equiv \mu_g - \mu_s$ is the chemical potential difference between the gas,

$$\mu_g = T \ln(N - N_s)/(\Omega - N_s) = T \ln n_g \ , \tag{10}$$

and the solid μ_s. The second derivative

$$\frac{\partial^2 \Delta F}{\partial N_s^2} = -(\bar{\gamma}/2) N_s^{-3/2} + T[(N - N_s)^{-1} - (\Omega - N_s)^{-1}] \tag{11}$$

is positive when $N_s \to N$ and is negative when $N_s \to 0$. Thus if Eq. (9) has solutions, ΔF has two extrema: one maximum at a small $N_s^{(1)}$ and one minimum at a large $N_s^{(2)}$ as is shown in Fig. 3(a). In a closed and small system, the crystal takes a size $N_s^{(2)}$ which corresponds to the minimum of the free-energy cost ΔF, if $\Delta F(N_s^{(2)}) < 0$. As $|\mu_s|$ decreases, $N_s = 0$ becomes the absolute minimum position of a free energy, and $N_s^{(2)}$ corresponds only to a metastable state. Finally, when $|\mu_s|$ becomes smaller than the critical value $\mu_{s,c}$ where $\partial \Delta F/\partial N_s = \partial^2 \Delta F/\partial N_s^2 = 0$, only the gas phase is stable and the crystal nucleus should evaporate. The relation between the crystal size N_s and the chemical potential $|\mu_s|$ at $T/J = 0.3$ is shown in Fig. 3(b). The data points obtained by simulation lie quite close to a theoretical curve given by Eq. (9). Furthermore, when we initiate a simulation with a small initial nucleus of the size N_s which lies to the left of the unstable branch in Fig. 3(b), the solid nucleus evaporates completely. Also, if the simulation is done with a chemical potential $|\mu_s|$ smaller than the critical value, the solid nucleus again evaporates and extin-

guishes. All these facts confirm the μ_s versus N_s relation in Fig. 3(b).

For a given solid chemical potential μ_s and a given gas chemical potential μ_g, or equivalently, a gas density $n_g=(N-N_s)/(\Omega-N_s)$, a crystal nucleus with a size $N_s=(\bar{\gamma}/\Delta\mu)^2$ corresponds to the stationary point of ΔF. When one increases the system size Ω and the total number of atoms N so as to keep n_g constant, N_s remains the extremum of ΔF. However, its stability changes when N exceeds the threshold value $N_{\rm th}$ determined from the relation $\partial\Delta F/\partial N_s=\partial^2\Delta F/\partial N_s^2=0$: The threshold values of N and Ω are

$$N_{\rm th}=N_s\left[1+\frac{2(1-n_g)}{\Delta\mu/T}\right],$$
$$\Omega_{\rm th}=N_s\left[1+\frac{2(1-n_g)}{n_g\Delta\mu/T}\right]. \tag{12}$$

For a small system with $\Omega<\Omega_{\rm th}$ and $N<N_{\rm th}$, the crystal nucleus with a size N_s is stable, whereas for a large system with $\Omega>\Omega_{\rm th}$ and $N>N_{\rm th}$, it becomes unstable. Thus for an open system where the volume Ω and the total number of atoms N are infinite with a fixed gas density $n_g=N/\Omega$, a crystal nucleus with a size N_s larger than a critical size $N_{s,c}=(\bar{\gamma}/\Delta\mu)^2$ should grow.

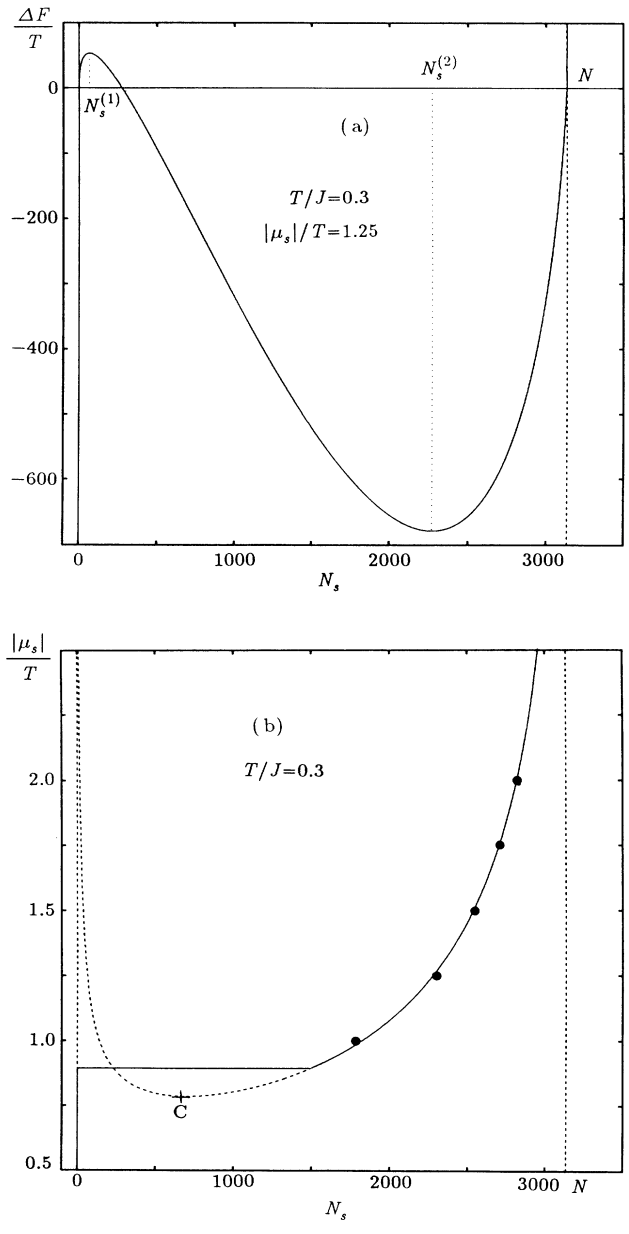

FIG. 3. (a) Free-energy cost ΔF for the formation of a crystal nucleus with a size N_s. The system size is $\Omega=70\times70$, the total atom number is $N=56\times56$, the temperature is $T/J=0.3$, and the chemical potential is $|\mu_s|/T=1.25$. (b) Chemical potential $|\mu_s|/T$ vs the equilibrium values of the nucleus size N_s. Closed points represent simulation results, a solid curve the stable branch, and a dashed curve the metastable and the unstable branches. C represents a critical point.

III. GROWTH SHAPE

A. Simulation of an open system

In an open system where Ω and N are infinite the crystal grows. In order to measure a time, we introduce a time unit such that a single diffusion trial of a gas atom corresponds to a time increment of $\Delta t=(4N_g)^{-1}$ when there are N_g gas atoms. By choosing the lattice parameter as a unit of length, the diffusion constant D then reduces to unity. Since the diffusion process is independent of the solidification and evaporation processes, their time constants, τ_D and $\tau_{\rm SE}$, can be chosen arbitrarily. In this paper we set $\tau_D=\tau_{\rm SE}=1$. We prepare list of the gas and the interfacial solid atoms, and select an atom from the list randomly. If it is a gas atom, diffusion is tried, and if its new position is next to the solid atom, solidification is tried. If the one selected is a solid atom, evaporation is tried. Therefore, in a time increment of $\Delta t=\frac{1}{4}$, each gas atom tries diffusion as well as solidification if possible, and each solid atom on the interface tries evaporation once on the average. The vessel is assumed to have a circular shape in order to lessen an anisotropy in the diffusion field.

Simulation is performed at a very low temperature as $T/J=0.3$. The gas density is fixed rather high to be $n_g=0.5$ in order to make scales of length and time short enough for practical simulation. When a chemical potential μ_s is set smaller than $\mu_g=T\ln n_g=-0.69T$, the density n_g is higher than the thermodynamic equilibrium gas density $n_{g,\rm eq}=e^{\mu_s/T}$. The crystal is thus surrounded by a supersaturated gas. By setting an initial size of a crystal nucleus larger than the critical one $(\bar{\gamma}/\Delta\mu)^2$, and the initial system size larger than the threshold value $\Omega_{\rm th}$, the crystal starts to grow.

For a continuous growth of the crystal, we provide a particle reservoir at the periphery of the vessel, which is a thin region of a fixed gas density. The reservoir should be

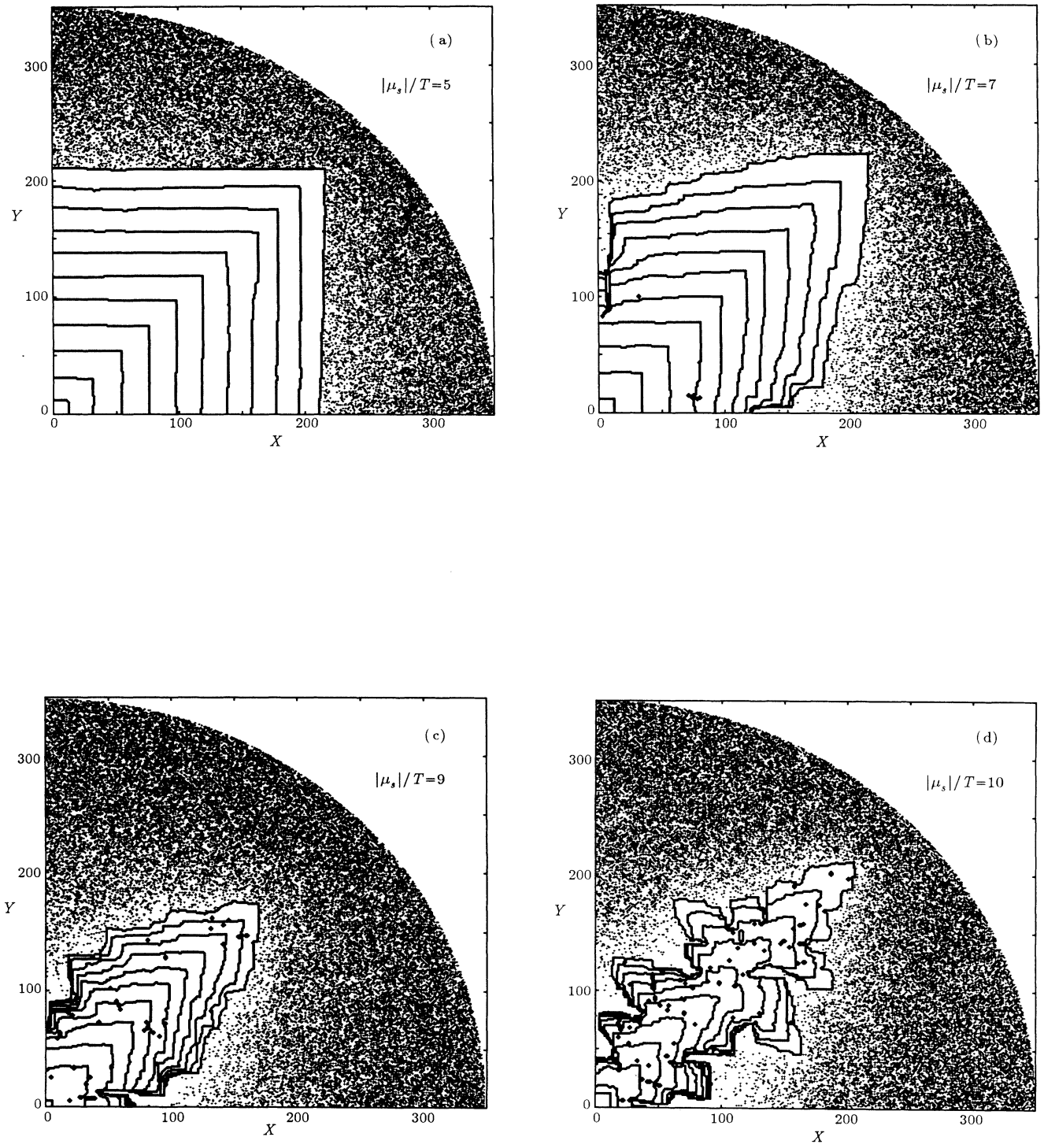

FIG. 4. Stroboscopic growth shapes of the crystal at various μ_s's, and gas atoms distributed around the final configuration of the crystal. Chemical potential $|\mu_s|/T$ is (a) 5.0, (b) 7.0, (c) 9.0, (d) 10.0, (e) 11.0, (f) 12.0, (g) 13.0, and (h) ∞. For (g) and (h) only the final crystal shape is shown in black, and in (h) gas atoms are omitted.

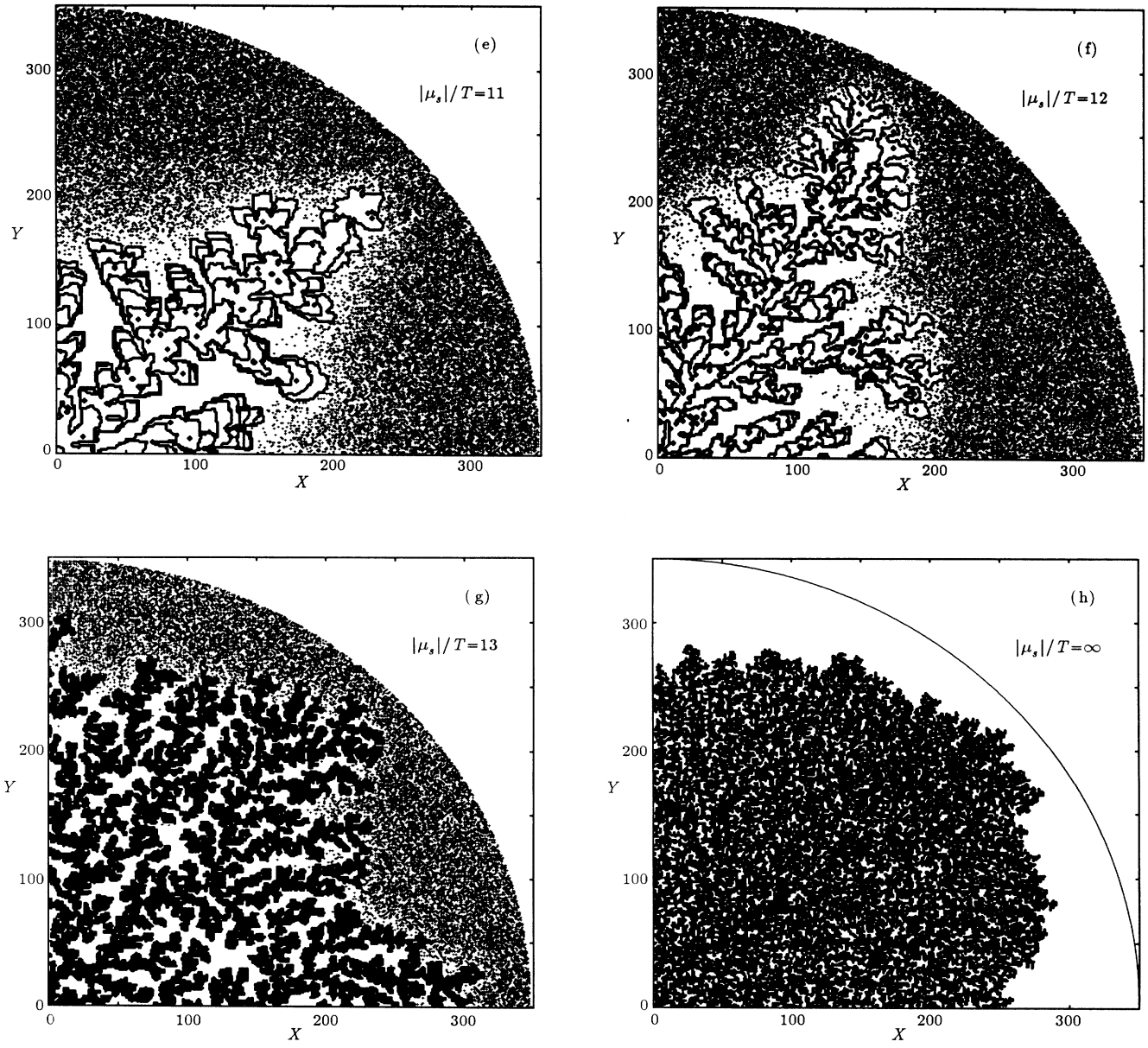

FIG. 4. (*Continued*).

set far enough from the interface in order not to disturb the gas-density distribution. When the crystal grows, it absorbs surrounding gas atoms and the density around the crystal is suppressed. The natural length scale that characterizes the variation of the diffusion field is the diffusion length $l=2D/V$, where V is the growth velocity. The best way to shift the particle reservoir outwardly is, therefore, to keep its separation from the crystal tip larger than l. This scheme is applicable at high $|\mu_s|/T$. At small $|\mu_s|$, however, the crystal grows very slowly and the diffusion length $l=2D/V$ is very large. In order to keep the system small enough to perform simulation, we choose another scheme: The particle reservoir is shifted outwardly only when the density in front of this region is depressed more than the level of random fluctuation from the prescribed value. Since the growth at these small $|\mu_s|$ will turn out to be strongly governed by the interface kinetics, we expect that our scheme of the reservoir shift may not influence the growth kinetics essentially. At $|\mu_s|/T=8.0$, simulations with different schemes in shifting the reservoir yield similar shape evolution, and the velocities agree with each other [Fig. 5(a)].

B. Structure and dynamics

Simulated growth shapes of the crystal vary on increasing the energy gain $|\mu_s|/T$ associated with the solidification, as is shown in Fig. 4. At small $|\mu_s|/T$

$=4.0$ and 5.0, the crystal grows slowly and its shape is polygonal up to our maximum simulation size [Fig. 4(a)]. On increasing $|\mu_s|/T$ from 6.0 to 10.0, the crystal grows initially in a square form, but becomes unstable at the corner, and turns into a dendritic form ultimately [Figs. 4(b)–4(d)]. A further increase in $|\mu_s|/T$ leads to the splitting of the dendritic tip and many irregular branches are observed [Figs. 4(e) and 4(f)]. Until $|\mu_s|/T=12$, the structure is rather open, but from $|\mu_s|/T \geq 13$ the width and the spacing between dendritic branches become very fine and the whole structure looks compact. [Figs. 4(g) and 4(h)].

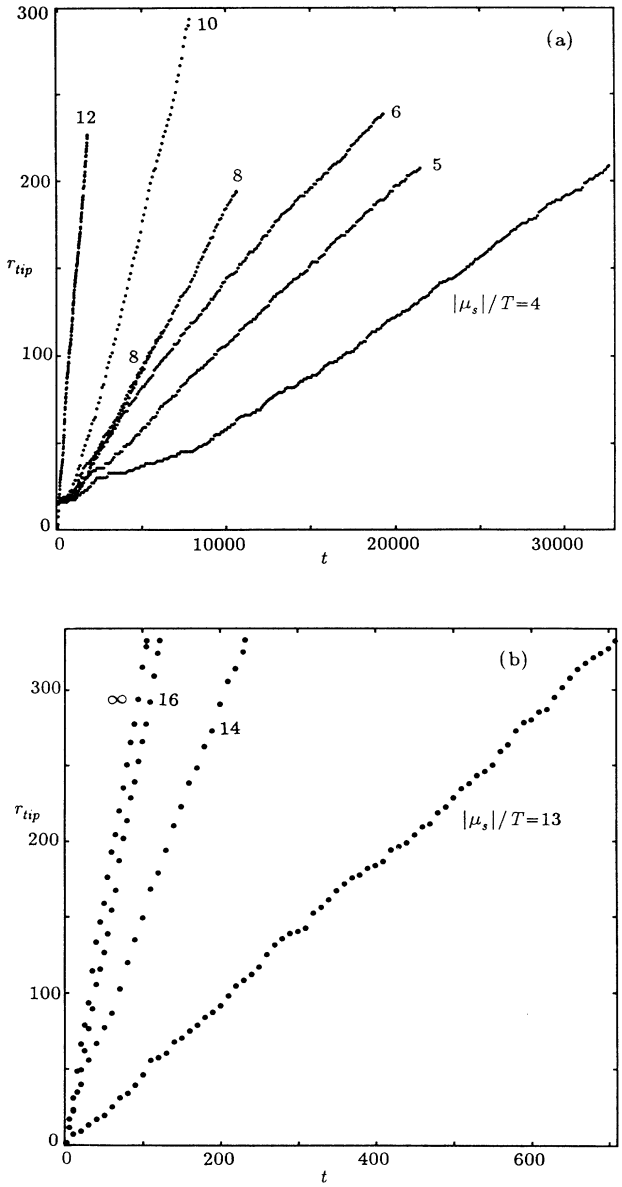

FIG. 5. Time evolution of the crystal size r_{tip} at (a) small and (b) large chemical potentials. At $|\mu_s|/T=8.0$ two different schemes in shifting the gas reservoir yield almost identical behavior.

As for the dynamical aspects of the crystal growth, time evolution of the crystal tip is observed. A separation r_{tip} of the farthest tip of the crystal from the origin increases asymptotically in proportion to the time t, as is shown in Fig. 5. At $|\mu_s|/T=8.0$, the r_{tip}'s for two different schemes in shifting the particle reservoir at the periphery of the vessel increase almost identically, as shown in Fig. 5(a). The growth rate is defined by the time variation of r_{tip} as $V=\Delta r_{tip}/\Delta t$. The chemical potential dependence of V is shown in Fig. 6(a). When the crystal grows in a square form or in an open dendritic form, the growth rate is very small. On the other hand, when the crystal grows in a compact form its growth rate increases drastically. The logarithmic plot of the rate V in Fig. 6(b) reveals that for small $|\mu_s|$'s V depends exponentially on $|\mu_s|/T$ as

$$V \propto \exp(-0.29|\mu_s|/T) . \tag{13}$$

Figure 6(b) also shows a smooth increase of the velocity V around $|\mu_s|/T=8$, tracing no hint of difference in the shifting scheme of the reservoir there, above and below. It confirms again the validity of our simulation procedure.

C. Nucleation growth at small $|\mu_s|$

In order to characterize the crystal structure at small $|\mu_s|$, we estimate the stability limit of the square crystal L_{max}. When a crystal grows in a square form, the number of surface crystal atoms $N_{s,i}$ is equal to $2L-1$, with $L=\sqrt{N_s}$ being the linear dimension of the square crystal of a size N_s. When a crystal becomes dendritic, the interface becomes complicated and the ratio between $N_{s,i}$ and L increases: If, for example, a dendritic branch grows with a constant width, $N_{s,i}$ is proportional to the total number N_s. This expectation is clearly seen in Fig. 7, which depicts $(N_{s,i}+1)/2L$ versus L. For small $L<L_{max}$, the ratio remains unity, while for $L>L_{max}$ the ratio increases rapidly. The stability limit L_{max} thus obtained is plotted in Fig. 8 as a function of the chemical potential $|\mu_s|$. From this plot one observes that L_{max} also depends exponentially on the chemical potential $|\mu_s|$. The least-squares fit leads to the relation

$$L_{max} \propto \exp(-0.59|\mu_s|/T) . \tag{14}$$

When the crystal grows larger than L_{max}, it takes a dendritic profile. The tip size and the sidebranch periodicity of the dendritic structure still seem to be scaled with L_{max}, as shown in Fig. 4. Thus L_{max} characterizes the structure in the crystal.

One thing to note is that the morphological transition from polygonal to hopper or dendritic structure induces a drastic increase in the time evolution of $N_{s,i}$, but not in the tip velocity, as is shown in Fig. 5. The tip velocity shows only a transient slow evolution in time. The reason may be that the tip velocity is mainly determined by a local environment, such as gas-density distribution, which does not change so much, even when global morphology varies.

The exponential dependence of V and L_{max} on $|\mu_s|$

may be interpreted by the surface kinetics of the nucleation and growth mechanism. For a small $|\mu_s|$ a crystallization probability of an isolated atom on an edge site is very low as

$$P_1 = n_{g,i}\exp[(|\mu_s|-4J)/T]/\{1+\exp[(|\mu_s|-4J)/T]\}$$
$$\approx n_{g,i}\exp[(|\mu_s|-4J)/T] \ . \quad (15)$$

Here $n_{g,i}$ is the gas density at the interface, and $4J$ represents the energy cost to create two excessive broken bonds. Once a solid atom is nucleated on the flat edge, further spreading costs no energy and a layer growth takes place quickly. Since the total probability of nucleation on an edge of the length $2L$ is $2LP_1$, the growth rate of an edge is obtained to be

$$V_K = 2LP_1 \ . \quad (16)$$

In the steady state, gas atoms consumed by the nucleation and growth should be supplied through the diffusion in the gas phase. The surface kinetics rate V_K

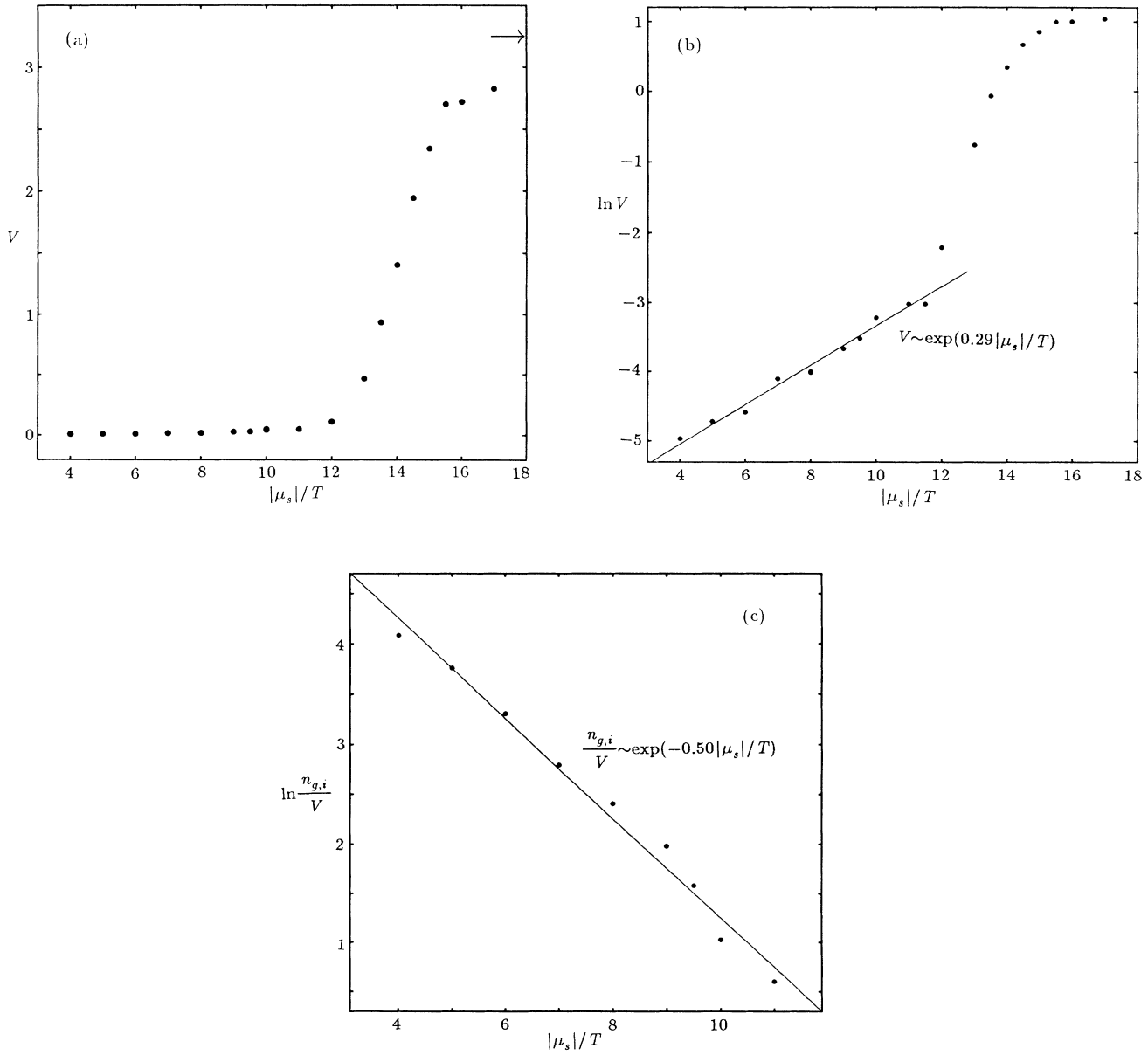

FIG. 6. (a) Steady growth rate V vs chemical potential. An arrow indicates the velocity at $|\mu_s| = \infty$. (b) $\ln V$ vs $|\mu_s|/T$. A straight line shows the least-squares fit. (c) $\ln(n_{g,i}/V)$ vs $|\mu_s|/T$. A straight line shows the least-squares fit.

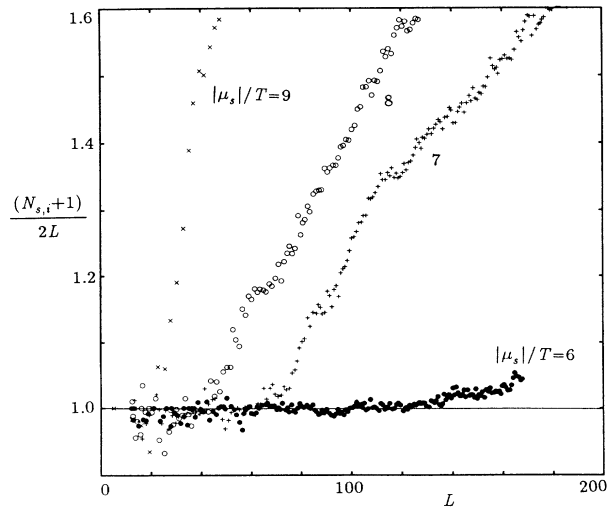

FIG. 7. Ratio between the numbers of the interfacial solid atoms $N_{s,i}$ and the linear dimension of the square crystal $L=\sqrt{N_s}$.

should be balanced with the diffusional rate V_D, and $V_K=V_D=V/\sqrt{2}$, where V is the growth rate in the diagonal direction. When the gas with density $n_{g,i}$ crystallizes into a solid with density $n_{s,i}$, at the interface, the mass deficiency produced per time $(n_{s,i}-n_{g,i})V_D$ should be transported via the diffusional flow $Dq \equiv D\partial_n n_g$, where ∂_n represents the normal gradient at the interface:

$$(n_{s,i}-n_{g,i})V_D=Dq \ . \tag{17}$$

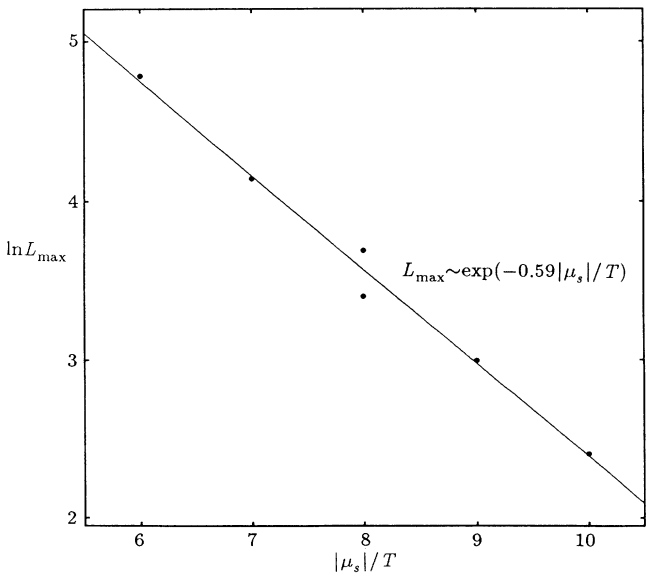

FIG. 8. Linear size of the stability limit for the polygonal growth $L_{\max}$ vs $|\mu_s|/T$. A straight line shows the least-squares fit.

Since $n_{s,i}=1$ and is much larger than $n_{g,i}$, we may replace the coefficient on the left-hand side to be unity. Until now we have assumed that the gas density along the polygonal edge $n_{g,i}$ is uniform. However, when the crystal grows steadily in the polygonal form, the density difference is produced between the corner and the center of the edge.[25–28] Since the density variation is characterized by diffusion length $l=2D/V$, the density difference between the corner, $n_g(\mathrm{L})$, and the center points, $n_g(0)$, is of order L/l, where L is half the edge length. Precise calculation[26] has been done with the static approximation to the diffusion field and the result is

$$n_g(L)-n_g(0)=(qL/\pi)[\psi(\tfrac{3}{4})-\psi(\tfrac{1}{2})]=0.28qL \ , \tag{18}$$

with ψ being the digamma function: $\psi(z)=d\ln\Gamma(z)/dz$.[29] Since $q\approx V_D/D\approx\sqrt{2}/l$, our qualitative argument is valid with a modification of a constant factor of the order unity. When the density at the center $n_g(0)$ is suppressed to the corresponding equilibrium density $n_{g,\mathrm{eq}}=e^{-|\mu_s|/T}(\ll 1)$, the central part cannot grow any more.[27] This determines the limit of polygonal growth for our model system. The maximum linear size $L_{\max}$ of the polygonal growth is obtained from Eqs. (16) and (18) to be

$$L_{\max}\sim\sqrt{n_{g,i}/P_1}\propto\exp[(4J-|\mu_s|)/2T] \ , \tag{19}$$

and the velocity is

$$V\sim\sqrt{n_{g,i}P_1}\propto n_{g,i}\exp[(|\mu_s|-4J)/2T] \ , \tag{20}$$

where we have approximated $n_g(L)=n_{g,i}$ and $n_g(0)=0$.

From Eq. (19) one expects $\ln L_{\max}$ to be proportional to $-|\mu_s|/2T$, which differs not so much from the simulated slope -0.59. For the growth rate V the comparison is not straightforward, since the gas density at the tip $n_{g,i}$ also varies as a function of μ_s, as is clear from the particle configurations in Fig. 4. In order to estimate $n_{g,i}$, we assume that the diffusion field around the growing tip varies exponentially with the diffusion length $l=2D/V$,

$$n_g(r)=n_g+(n_g-n_{g,i})\exp(-rV) \ . \tag{21}$$

Here $n_g=0.5$ is the gas density at infinity. We obtain from the simulation an average density $\bar{n}$ in the circle of radius a, which is approximately related to the gas density at the interface $n_{g,i}$ as

$$n_{g,i}=n_g-(n_g-\bar{n})(aV)^2/2[1-(1+aV)e^{-aV}] \ . \tag{22}$$

The interfacial gas density $n_{g,i}$ is then calculated from Eq. (22) and is found to depend on $|\mu_s|$ exponentially as

$$n_{g,i}\propto\exp(-0.22|\mu_s|/T) \ , \tag{23}$$

as shown in Fig. 9. The logarithm of the ratio $n_{g,i}/V$ at small $|\mu_s|/T$ is shown in Fig. 6(c), and is proportional to $|\mu_s|/T$ with the slope -0.50,

$$n_{g,i}/V\propto\exp(-0.50|\mu_s|/T) \ . \tag{24}$$

It may be fortuitous, but the slope just fits the expected value $-\frac{1}{2}$ in Eq. (20).

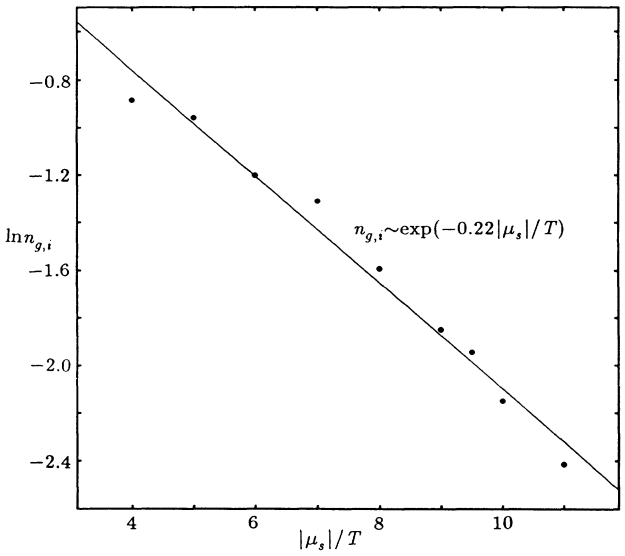

FIG. 9. Gas density at the interface tip $n_{g,i}$ obtained from the configuration. A straight line shows the least-squares fit.

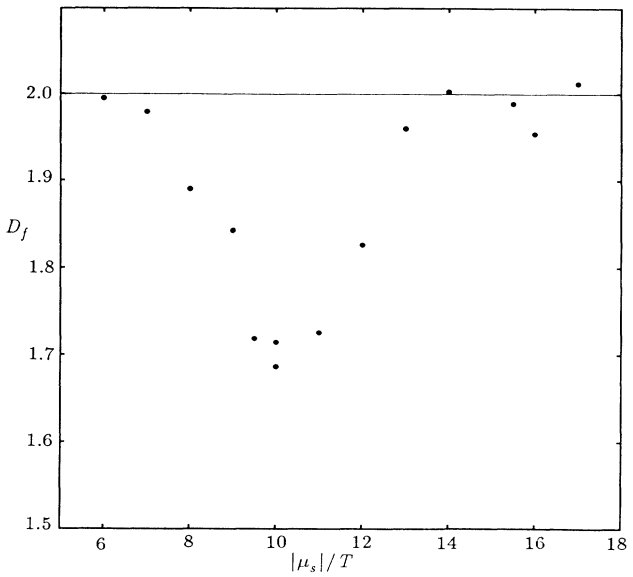

FIG. 10. Fractal dimension D_f of the crystal vs chemical potential $|\mu_s|/T$.

D. Irregular structure at high $|\mu_s|$'s

Up to the chemical potential $|\mu_s|/T \leq 10$, the system consists of a single primary dendrite, whereas for high $|\mu_s|/T \geq 11$ multiple branches are observed. This variation in morphology may be caused by the relative magnitude of the system size and the diffusion length $l = 2D/V$, which characterizes the density depression in the gas phase and also the separation between each dendrite. At small $|\mu_s|$'s with low growth rate, l is large and of the order of the system size, and the crystal cannot grow in an open space. At large $|\mu_s|$'s, on the other hand, l becomes short and the crystal can grow in an open space between primary dendrites. The open structure of the crystal is reflected in the relation between the mass N_s and the radius of gyration R_g, defined by

$$R_g^2 = (1/N_s) \sum_{i=1}^{N_s} r_i^2 , \tag{25}$$

where r_i is the distance of the ith solid atom from the origin. The relation

$$N_s \propto R_g^{D_f} \tag{26}$$

defines the fractal dimension[7] D_f. We have estimated D_f at various $|\mu_s|$'s, as is shown in Fig. 10, and obtained the value around 1.7 for the dendritic growth. The fractal dimension is near the value of the DLA, but the dendrite here is almost regular. D_f smaller than the space dimension $d = 2$ does not necessarily mean the irregular fractal structure but merely represents the openness of the structure. Since the sidebranch of the dendrite develops while the primary dendrite elongates, D_f turns out to be larger than 1.

For $|\mu_s|/T$ higher than $13 \approx 4J/T$, the energy barrier against nucleation given in Eq. (15) vanishes and most gas atoms solidify when they attach to the solid. The velocity V increases drastically compared to the nucleation growth rate at small $|\mu_s|$'s. The diffusion length is less than unity, and the structure in the growth form becomes very fine. The fractal dimension D_f of the aggregate agrees now with the space dimension $d = 2$, indicating that the system is "compact."[30] Even though D_f is equal to $d = 2$ both at very small and very large $|\mu_s|$'s, the crystal structure is quite different: polygonal structure at small $|\mu_s|$'s and irregular compact structure at large $|\mu_s|$'s. The difference can be detected in the number of the interfacial solid atoms $N_{s,i}$. The relation between $N_{s,i}$ and the total number of the solid atoms N_s is asymptotically represented by the power law

$$N_{s,i} \propto N_s^{\alpha} . \tag{27}$$

Figure 11 depicts the variation of the exponent α as a function of the solid chemical potential $|\mu_s|/T$. At a small $|\mu_s|$, α takes the value $\frac{1}{2}$, representing that the shape is polygonal. At large $|\mu_s|$, α becomes 1, representing that the shape is complicated and that a finite fraction of solid atoms is situated at the interface. From $|\mu_s|/T = 11$ to 14, the value of α exceeds unity, indicating that the crossover from a polygonal to an irregular growth form is taking place gradually at about our system size.

When $|\mu_s|$ is infinite, a gas atom solidifies instantaneously as it touches the solid aggregate. The problem is the same with the DLA model growing in a gas with a finite density,[30] and the growth rate takes a maximum value $V_{\max}$. The assumption of a short diffusion length permits ample gas atoms around the crystal tip, and the

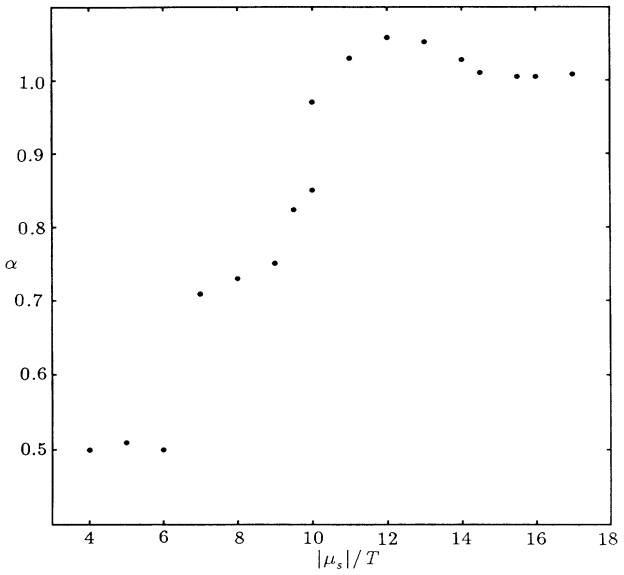

FIG. 11. Exponent α, which relates the number of interfacial solid atoms $N_{s,i}$ to that of the total solid atoms N_s as $N_{s,i} \propto N_s^{\alpha}$.

growth is essentially controlled by the surface kinetics. One can then estimate a rough value of the maximum velocity $V_{\max}$. When a diagonal site solidifies, the tip grows a distance of $\sqrt{2}$. In a time interval of $\Delta t = 1$, the site tries to crystallize four times in our choice of time unit. The probability of crystallization is equal to the probability of finding a gas atom on that site, which is about n_g. Therefore the growth rate is roughly estimated to be $V = \sqrt{2} \times 4 \times n_g \approx 2.8$ for our system with $n_g = 0.5$. The diffusion causes the rearrangement of gas atoms around the growing tip, and enhances the growth rate. The simulation result $V_{\max} = 3.25$ agrees with this estimation. The diffusion length $l = 2D/V \sim 0.6$ is less than the lattice parameter, and the assumption of the surface kinetics control is confirmed. The rate $V_{\max} = 3.25$ is a little smaller than, but of the same order of, the value $V = 3.64$ obtained in the growth simulation from a linear seed of the solid.[30] Since in Ref. 30 solidification is tried before and after the diffusion, crystallization is more favored and a higher growth rate comes out than in the present work.

IV. SUMMARY AND DISCUSSIONS

Crystal shapes are simulated by using a lattice-gas model, which incorporates the surface tension of the solid, chemical potentials of the solid and the gas phases, and also the diffusion dynamics in the gas phase. Simulations for a closed system at various temperatures produce equilibrium shapes on a square lattice, which agree with the exact profiles of the corresponding Ising model. The crystal size also agrees with the prediction from the free-energy minimization analysis.

By extending the simulation to an open system which is provided with a particle reservoir with a fixed gas density, various growth shapes are obtained. On decreasing the solid chemical potential $\mu_s (< 0)$, the growth shape changes from a polygonal through a hopper to a dendrite, and then to a fractal aggregate, and finally to an irregular but compact structure. This kind of variation is realized in the growth experiment of the cyclohexanol crystal from pure melt.[31] Morphological transitions are studied in other systems, such as in electrochemical deposition[32,33] and in viscous fingers in a radial Hele-Shaw cell with some anisotropies.[34,35] Especially, in a Hele-Shaw cell with a regular sixfold lattice of grooves ruled on the bottom plate, apparently similar morphological transitions are observed.[34] On increasing pressure, faceted growth varies to dendritic growth. At higher pressure, tips split, which on further increase of pressure stabilize again to form dendrites. Two dendrites at low and high pressures are rotated 30° mutually, and the intermediate tip splitting is due to the competition between selective orientations of different dendrites. In our lattice-gas model, tip splitting and irregularity are caused by the random shot noise by the solidification, like the DLA model. Therefore, in spite of the apparent similarity, morphology diagrams may be determined differently in two cases.

Crystal growth at small $|\mu_s|$ is characterized by the exponential dependence of the maximum size of the polygonal crystal $L_{\max}$ on $-|\mu_s|/T$. The ratio $n_{g,i}/V$ between the interfacial gas density $n_{g,i}$ and the growth rate V also shows similar dependence on μ_s. These results can be interpreted by the single nucleation and growth mechanism on the edge of a crystal. However, we do not yet have a proper explanation for the $\Delta\mu$ dependence of V and $n_{g,i}$, respectively. According to the static approximation of the diffusion field,[26] gas densities at the corner and the center of the edge are obtained as

$$n_g(L) = n_g - 0.27qL, \quad n_g(0) = n_g - 0.55qL \ . \tag{28}$$

For $|\mu_s|/T \gg 1$, the assumption of the small equilibrium density at the center yields the constant gas density at the corner $n_{g,i} = n_g(L) \approx n_g/2$ and the chemical potential dependence of the growth rate as

$$V = Dq \sim n_g / L_{\max} \propto \exp(-|\mu_s|/2T) \ .$$

These results disagree with the simulation results, Eqs. (13) and (23). It may be necessary to take the time variation of the diffusion equation into account.

When the crystal grows larger than $L_{\max}$, it becomes dendritic. The main structures such as the tip width and the sidebranch periodicity still seems to be governed by the scale $L_{\max}$. The dendritic crystal has a rather open structure, which is characterized by its fractal dimension D_f about 1.7. Further increase in $|\mu_s|$ lets the crystal grow fast, such that the diffusion length l becomes comparable to or less than the lattice parameter. In this case, the crystal becomes compact with $D_f = d = 2$. Even though both the polygonal and the compact crystals have the same D_f, their structures are completely different: The number of interfacial solid atoms $N_{s,i}$ is a fraction of the total solid atoms N_s for the irregular crystal, whereas it is proportional to the linear size $L = \sqrt{N_s}$ for the polygonal crystal.

We have to remark that the characterization of the growth shapes depends on the crystal size. Even for small $|\mu_s|$'s such as $|\mu_s|/T=4.0$ and 5.0, the dendritic instability may appear when the crystal becomes larger than the corresponding $L_{\max}$. Also at $|\mu_s|/T \lesssim 10.0$ when the dendrite grows larger than the diffusion length, a secondary branch might evolve to fill in the open space between main branches. These points are, however, out of our computation capability. Effects of the temperature, of the ratio of τ_D and τ_{SE}, and of the surface diffusion are the interesting future problems to be studied.

ACKNOWLEDGMENTS

Y.S. is grateful to Dr. M. Uwaha for valuable discussions and for a critical reading of the manuscript. The study is partially financed by a Grant-in-Aid from the Ministry of Education, Science and Culture, Japan, and also by the Keio-Gijuku Academic Development Funds.

[1]J. S. Langer, Rev. Mod. Phys. **52**, 1 (1980).
[2]R. Trivedi, Metal. Trans. **15A**, 977 (1984).
[3]S. C. Huang and M. E. Glicksman, Acta Metall. **29**, 701 (1981); **29**, 717 (1981).
[4]R. G. Saffman and F. R. S. G. Taylor, Proc. R. Soc. London, Ser. A **245**, 312 (1958).
[5]L. Paterson, J. Fluid Mech. **113**, 513 (1981).
[6]E. Ben-Jacob, G. Deutscher, P. Garik, N. D. Goldenfeld, and Y. Lareah, Phys. Rev. Lett. **57**, 1903 (1986).
[7]T. A. Witten and L. M. Sander, Phys. Rev. Lett. **47**, 1400 (1981); Phys. Rev. B **27**, 5686 (1983).
[8]E. Ben-Jacob, N. D. Goldenfeld, J. S. Langer, and G. Schön, Phys. Rev. Lett. **51**, 1930 (1983); Phys. Rev. A **29**, 330 (1984).
[9]D. A. Kessler, J. Koplik, and H. Levine, Phys. Rev. A **30**, 3161 (1984); Adv. Phys. **37**, 255 (1988).
[10]B. Caroli, C. Caroli, B. Roulet, and J. S. Langer, Phys. Rev. A **33**, 442 (1986).
[11]A. Barbieri, D. C. Hong, and J. S. Langer, Phys. Rev. A **36**, 3340 (1987).
[12]Y. Saito, G. Goldbeck-Wood, and H. Müller-Krumbhaar, Phys. Rev. Lett. **58**, 1541 (1987); Phys. Rev. A **38**, 2148 (1988).
[13]A. Karma, Phys. Rev. Lett. **57**, 858 (1986); Phys. Rev. A **34**, 4353 (1986).
[14]T. Dombre and V. Hakim, Phys. Rev. A **36**, 2811 (1987); M. Ben Amar and B. Moussallam, Phys. Rev. Lett. **60**, 317 (1988).
[15]Y. Saito, C. Misbah, and H. Müller-Krumbhaar, Nucl. Phys. B (Proc. Suppl.) **5A**, 225 (1988).
[16]B. I. Shraiman, Phys. Rev. Lett. **56**, 2028 (1986); D. C. Hong and J. S. Langer, *ibid.* **56**, 2032 (1986); R. Combescot, T. Dombre, V. Hakim, Y. Pomeau, and A. Pumir, *ibid.* **56**, 2036 (1986).
[17]T. Vicsek, Phys. Rev. A **32**, 3084 (1985).
[18]J. D. Weeks, in *Ordering in Strongly Fluctuating Condensed Matter Systems,* edited by T. Riste (Plenum, New York, 1980), p. 293.
[19]C. Rottman and M. Wortis, Phys. Rev. B **29**, 328 (1984).
[20]*Monte Carlo Methods in Statistical Physics,* edited by K. Binder (Springer, Berlin, 1979).
[21]Y. Saito and M. Uchiyama, in Proceedings of the Oji International Seminar of Morphology and Growth Unit of Crystals, Yamagata, Japan, 1985 (unpublished).
[22]Y. Akutsu and N. Akutsu, J. Phys. Soc. Jpn. **56**, 9 (1987).
[23]A. F. Andreev, Zh. Eksp. Teor. Fiz. **80**, 2042 (1981) [Sov. Phys.—JETP **53**, 1063 (1982)].
[24]C. Rottman and M. Wortis, Phys. Rev. B **24**, 6274 (1981).
[25]W. F. Berg, Proc. R. Soc. London, Ser. A **164**, 79 (1938).
[26]A. Seeger, Philos. Mag. Ser. 7 **44**, 1 (1953).
[27]J. W. Cahn, in *Crystal Growth,* edited by H. S. Peiser (Plenum, Oxford, 1966), p. 681.
[28]T. Kuroda, T. Irisawa, and A. Ookawa, J. Cryst. Growth **42**, 41 (1977).
[29]*Handbook of Mathematical Functions,* edited by M. Abramowitz and I. A. Stegun (Dover, New York, 1972), p. 258.
[30]M. Uwaha and Y. Saito, J. Phys. Soc. Jpn. **57**, 3285 (1988); Phys. Rev. A (to be published).
[31]R. E. Ovsienko, A. Alfintsev, and V. V. Maslov, J. Cryst. Growth **26**, 233 (1974).
[32]Y. Sawada, A. Dougherty, and J. P. Gollub, Phys. Rev. Lett. **56**, 1260 (1986).
[33]D. Grier, E. Ben-Jacob, R. Clarke, and L. M. Sander, Phys. Rev. Lett. **56**, 1264 (1986).
[34]E. Ben-Jacob, R. Godbey, N. D. Goldenfeld, J. Koplik, H. Levine, T. Mueller, and L. M. Sander, Phys. Rev. Lett. **55**, 1315 (1985); E. Ben-Jacob, P. Garik, T. Mueller, and D. Grier, Phys. Rev. A **38**, 1370 (1988).
[35]A. Buka, J. Kertész, and T. Vicsek, Nature **323**, 424 (1986); A. Buka and P. Palffy-Muhoray, Phys. Rev. A **36**, 1527 (1987).